Inorg. Chem. **2006**, *45*, 3295–3300

The Mixed-Valent Manganese [3 × 3] Grid $[Mn(III)_4Mn(II)_5(2poap\text{-}2H)_6](ClO_4)_{10}\cdot 10H_2O$, a Mesoscopic Spin-$^1/_2$ Cluster

Oliver Waldmann,*,† Hans U. Güdel,† Timothy L. Kelly,‡ and Laurence K. Thompson‡

Department of Chemistry and Biochemistry, University of Bern, CH-3012 Bern, Switzerland, and Department of Chemistry, Memorial University of Newfoundland, St. John's, Newfoundland, A1B 3X7, Canada

Received November 30, 2005

The magnetic susceptibility and low-temperature magnetization curve of the [3 × 3] grid $[Mn(III)_4Mn(II)_5(2poap\text{-}2H)_6](ClO_4)_{10}\cdot 10H_2O$ (**1**) are analyzed within a spin Hamiltonian approach. The Hilbert space is huge (4 860 000 states), but the consequent use of all symmetries and a two-step fitting procedure nevertheless allows the best-fit determination of the magnetic exchange parameters in this system from complete quantum mechanical calculations. The cluster exhibits a total spin $S = {}^1/_2$ ground state; the implications are discussed.

Introduction

The magnetism of polynuclear complexes containing magnetic metal ions, often called molecular nanomagnets, has captured the imagination of chemists and physicists alike. In the chemical arena, the building of novel materials with a functionality of potential interest for applications from a "bottom up" approach has stimulated much effort. From the physical perspective, these nanometer-sized magnetic clusters have been demonstrated to exhibit many spectacular magnetic quantum phenomena.[1−4]

The understanding of the magnetic properties of clusters with multiple magnetic centers, which usually starts with an analysis of the temperature dependence of the magnetic susceptibility $\chi(T)$, is difficult with respect to the evaluation of the exchange coupling constants. On one hand, the structure of the complex at hand easily may suggest many exchange parameters in the microscopic spin Hamiltonian,[5] and frequently, even with the use of simplified models, this leads to a heavily overparametrized situation concerning the magnetic susceptibility. The only solution to this problem is to obtain information from several complementary experimental techniques. On the other hand, the dimension of the Hilbert space of the microscopic spin Hamiltonian increases exponentially with the spin dimension of the magnetic centers so that the (numerical) calculation of magnetic properties quickly reaches the limits of today's computers. This is particularly true for the calculation of $\chi(T)$, since at higher temperatures essentially all energy levels are thermally populated and hence contribute, so that the full energy spectrum needs to be calculated. This is in contrast to other techniques for determining the magnetic parameters, for example, inelastic neutron scattering, which typically are performed at low temperatures. Here, only a small number of the low-lying states is involved which with sparse-matrix diagonalization techniques can be obtained for systems orders of magnitude larger than those accessible by full diagonalization techniques.

In this work we analyze the magnetic susceptibility and low-temperature magnetization curve of the mixed-valent

* To whom correspondence should be addressed: E-mail: waldmann@iac.unibe.ch.
† University of Bern.
‡ Memorial University of Newfoundland.

(1) (a) Sessoli, R.; Gatteschi, D.; Caneschi, A.; Novak, M. A. *Nature (London)* **1993**, *365*, 141. (b) Gatteschi, D.; Sessoli, R. *Angew. Chem., Int. Ed.* **2003**, *42*, 268. (c) Friedman, J. R.; Sarachik, M. P.; Tejeda, J.; Ziolo, R. *Phys. Rev. Lett.* **1996**, *76*, 3830. (d) Thomas, L.; Lionti, F.; Ballou, R.; Gatteschi, D.; Sessoli, R.; Barbara, B. *Nature (London)* **1996**, *383*, 145. (e) Wernsdorfer, W.; Sessoli, R. *Science* **1999**, *284*, 133. (f) Wernsdorfer, W.; Aliaga-Alcalde, N.; Hendrickson, D. N.; Christou, G. *Nature (London)* **2002**, *416*, 406. (g) Hill, S.; Edwards, R. S.; Aliaga-Alcalde, N.; Christou, G.; *Science* **2003**, *302*, 7. (h) Del Barco, E.; Kent, A. D.; Yang, E. C.; Hendrickson, D. N. *Phys. Rev. Lett.* **2004**, *93*, 157202. (i) Waldmann, O.; Dobe, C.; Mutka, H.; Furrer, A.; Güdel, H. U. *Phys. Rev. Lett.* **2005**, *95*, 057202.
(2) Waldmann, O.; Guidi, T.; Carretta, S.; Mondelli, C.; Dearden, A. L. *Phys. Rev. Lett.* **2003**, *91*, 237202.
(3) Waldmann, O.; Carretta, S.; Santini, P.; Koch, R.; Jansen, A. G. M.; Amoretti, G.; Caciuffo, R.; Zhao, L.; Thompson, L. K. *Phys. Rev. Lett.* **2004**, *92*, 096403.
(4) Waldmann, O. *Coord. Chem. Rev.* **2005**, *249*, 2550.

(5) Unfortunately, there is no general consensus concerning the denotation for the various spin Hamiltonians (SH) which appear in the discussion of molecular nanomagnets. In this work, "microscopic SH" consistently refers to the SH which acts in the full spin space of the cluster, whereas a SH acting in a subspace of it is called an "effective SH".

10.1021/ic052055d CCC: $33.50
Published on Web 03/21/2006

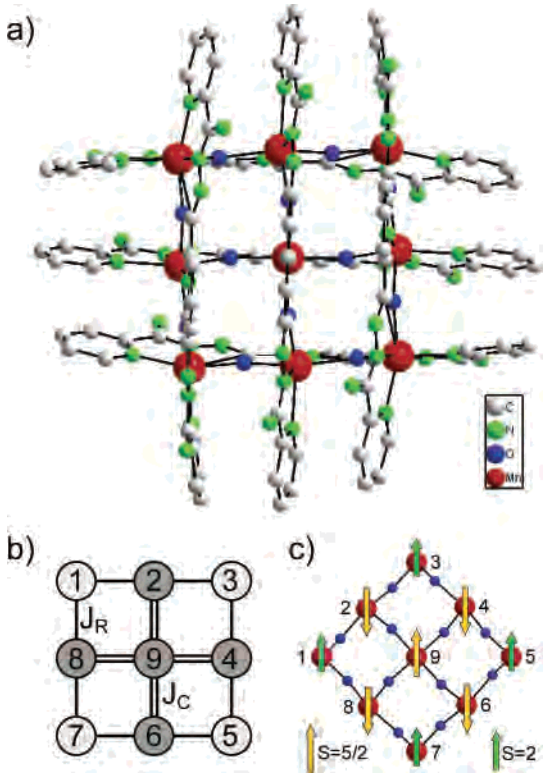

Figure 1. (a) Structural representation of the cation in **1**; (b) magnetic exchange model for **1**. The light-gray circles represent the spin-2 Mn(III) ions, and the dark-gray circles represent the spin-$^5/_2$ Mn(II) ions. (c) The classical spin configuration of the $S = {}^1/_2$ ground state in **1** is shown.

manganese [3 × 3] grid $[Mn(III)_4Mn(II)_5(2poap\text{-}2H)_6](ClO_4)_{10}\cdot 10H_2O$ (**1**).[6,7] The structure is shown in Figure 1. The four spin-2 Mn(III) ions are located at the corners of the grid, whereas the remaining five metal sites are occupied by spin-$^5/_2$ Mn(II) ions. The Hilbert space of this cluster with its almost 5 million states is discouragingly large. We will show, however, that the subsequent use of all symmetries of the appropriate exchange Hamiltonian in combination with a two-step fitting procedure allows a reliable estimation of the exchange coupling parameters in this system (for the assumed exchange model see Figure 1b).

The experimental and theoretical analysis demonstrates that the antiferromagnetic interactions in **1** result in a total spin $S = {}^1/_2$ cluster ground state. This can be understood within a simple classical picture of the ground-state spin configuration in which the spin vectors on the Mn(III) sites and the central Mn(II) ion point up and the ones on the Mn(II) edge sites point down, accommodating the antiferromagnetic interactions best. Hence, $(4 \times 2) + {}^5/_2 - (4 \times {}^5/_2) = {}^1/_2$. Thus, the grid **1** is a rare example of a mesoscopic spin-$^1/_2$ cluster, in which the $S = {}^1/_2$ ground state arises from the concerted motion of many (magnetic) electrons. The prototypical example is the cluster V_{15}, in which 15 electrons couple to a (2-fold degenerate) $S = {}^1/_2$ ground state.[8] Another example is the Cr_7Ni molecule, in which 23 electrons act together to yield an $S = {}^1/_2$ ground state.[9,10] In **1**, the $S = {}^1/_2$ ground state is the result of 41 electrons interacting in a completely isotropic fashion within the antiferromagnetic grid structure. The interest in this special class of magnetic molecules comes from recent theoretical work, which suggests that such objects might be suitable for building qubits, the elementary building blocks in quantum computers (in this context they have been denoted as "antiferromagnetic cluster qubits").[11,12]

Experimental Section

$[Mn(III)_4Mn(II)_5(2poap\text{-}2H)_6](ClO_4)_{10}\cdot 10H_2O$ (**1**) was synthesized as reported.[6,7] The magnetic moment of powdered and polycrystalline samples was measured with an MPMS5 SQUID magnetometer (Quantum Design). The polycrystalline samples were produced by taking crystals out of the mother liquor and putting them directly into grease, in which they were crushed. This procedure minimizes potential problems due to drying of the sample through solvent loss and thus yields the most reliable magnetic data. However, the weight of the samples cannot be determined reliably, and the data were calibrated by matching the susceptibility at high temperatures to that of known powder samples. The accuracy of absolute values for the molar susceptibility and magnetic moments was estimated to be about 5%. Preliminary magnetic data were communicated previously.[6]

Results and Analysis

The temperature dependence of the susceptibility, as determined from a measurement at a field of 0.5 T, and the magnetization curve at 2 K are shown in Figure 2. The maximum in $\chi(T)$ at about 60 K clearly indicates antiferromagnetic interactions in the cluster, and the strong increase at the lowest temperatures indicates a ground state with $S > 0$. The $\chi(T)$ value at 250 K is 27.3 cm^3 K mol^{-1}, which is significantly lower than that of five spin-$^5/_2$ and four spin-2 ions (33.89 cm^3 K mol^{-1}). This further demonstrates the antiferromagnetic interactions. At low temperatures, $\chi(T)$ approaches a value of 0.42 cm^3 mol^{-1} indicative of an $S = {}^1/_2$ ground state (0.375 cm^3 K mol^{-1}). The magnetization curve at 2 K further supports an $S = {}^1/_2$ ground state. The continuing rise of the magnetization at higher fields suggests the presence of excited levels at about 10 K above the ground state.

On the basis of the grid structure, the magnetism of **1** should be well approximated by the microscopic spin

(6) Zhao, L.; Xu, Z.; Grove, H.; Milway, V. A.; Dawe, L. N.; Abedin, T. S. M.; Thompson, L. K.; Kelly, T. L.; Harvey, R. G.; Miller, D. O.; Weeks, L.; Shapter, J. G.; Pope, K. J. *Inorg. Chem.* **2004**, *43*, 3812.
(7) Thompson, L. K.; Kelly, T. L.; Dawe, L. N.; Grove, H.; Lemaire, M. T.; Howard, J. A. K.; Spencer, E. C.; Matthews, C. J.; Onions, S. T.; Coles, S. J.; Horton, P. N.; Hursthouse, M. B.; Light, M. E. *Inorg. Chem.* **2004**, *43*, 7605.
(8) (a) Müller, A.; Döring, J. *Angew. Chem., Int. Ed. Engl.* **1988**, *27*, 1721. (b) Gatteschi, D.; Pardi, L.; Barra, A. L.; Müller, A.; Döring, J. *Nature (London)* **1991**, *354*, 463. (c) Chiorescu, I.; Wernsdorfer, W.; Müller, A.; Bögge, H.; Barbara, B. *Phys. Rev. Lett.* **2000**, *85*, 3454.
(9) Larsen, F. K.; McInnes, E. J. L.; El Mkami, H.; Overgaard, J.; Piligkos, S.; Rajaraman, G.; Rentschler, E.; Smith, A. A.; Smith, G. M.; Boote, V.; Jennings, M.; Timco, G. A.; Winpenny, R. E. P. *Angew. Chem., Int. Ed.* **2003**, *42*, 101.
(10) Caciuffo, R.; Guidi, T.; Amoretti, G.; Carretta, S.; Liviotti, E.; Santini, P.; Mondelli, C.; Timco, G.; Muryn, C. A.; Winpenny, R. E. P. *Phys. Rev. B: Condens. Matter Mater. Phys.* **2005**, *71*, 174407.
(11) (a) Meier, F.; Levy, J.; Loss, D. *Phys. Rev. Lett.* **2003**, *90*, 047901. (b) Meier, F.; Levy, J.; Loss, D. *Phys. Rev. B: Condens. Matter Mater. Phys.* **2003**, *68*, 134417.
(12) Troiani, F.; Ghirri, A.; Affronte, M.; Carretta, S.; Santini, P.; Amoretti, G.; Piligkos, S.; Timco, G.; Winpenny, R. E. P. *Phys. Rev. Lett.* **2005**, *94*, 207208.

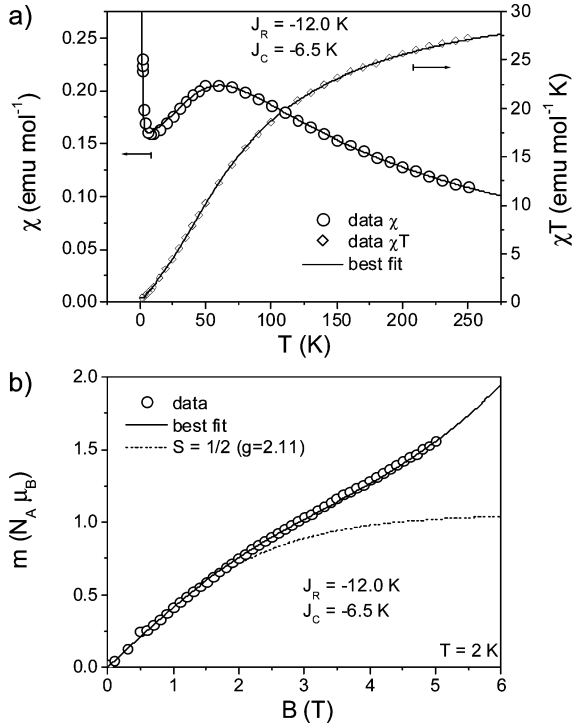

Figure 2. The open symbols show (a) the magnetic susceptibility versus temperature and (b) the magnetic moment versus applied field at 2 K of **1**. The solid line represents the best-fit results as calculated from Hamiltonian (1) with the exchange parameters as indicated, and the dashed line in part b represents the magnetization curve for an $S = {}^1/_2$ level.

Hamiltonian

$$H = -J_R\left(\sum_{i=1}^{7}\mathbf{S}_i\cdot\mathbf{S}_{i+1} + \mathbf{S}_8\cdot\mathbf{S}_1\right) - J_C(\mathbf{S}_2 + \mathbf{S}_4 + \mathbf{S}_6 + \mathbf{S}_8)\cdot\mathbf{S}_9 \quad (1)$$

where J_R describes the next-neighbor exchange interactions between the Mn(II) and Mn(III) ions on the grid periphery and J_C describes the interactions between the edge Mn(II) ions and the central Mn(II) ion. The $S = {}^1/_2$ ground state implies that both J_R and J_C are antiferromagnetic, that is, $J_R < 0$ and $J_C < 0$. Here $S_2 = S_4 = S_6 = S_8 = S_9 = {}^5/_2$ and $S_1 = S_3 = S_5 = S_7 = 2$. This corresponds to a [3 × 3] grid of five Mn(II) ions and four Mn(III) ions, with the Mn(III) ions located at the corners of the grid consistent with the structure. The dimension of the Hilbert space of this system is as large as 4 860 000. An exact (numerical) calculation of the energy spectrum, as required for the calculation and interpretation of the magnetic susceptibility data, is thus challenging, and one has to take advantage of the symmetries of the microscopic spin Hamiltonian as much as possible. The spin rotational symmetry of Hamiltonian (1) allows one to work with a spin level basis set, where each level is classified by the quantum numbers of the total spin, S and M. For Hamiltonian (1), the Hilbert space consists of a total of 398 400 spin levels, and the largest matrix to be diagonalized has a dimension of 49 995 (see Table 1). This still by far exceeds the capabilities of modern personal computers (a memory exceeding 23 GB would be required). However, the [3 × 3] grid structure exhibits an idealized D_4 spatial symmetry, which manifests itself as a D_4 spin permutational symmetry of Hamiltonian (1).[13] Accordingly, the basis functions can be chosen to also transform according to the irreducible representations A_1, A_2, B_1, B_2, and each of the components of E of the group D_4. A numerical efficient implementation of the spin permutational symmetry, however, is possible only for a coupling scheme of the spins which is left invariant under the operations of the group elements of D_4.[13] In the present case, this requirement is fulfilled, for example, for $\mathbf{S}_{15} = \mathbf{S}_1 + \mathbf{S}_5$, $\mathbf{S}_{37} = \mathbf{S}_3 + \mathbf{S}_7$, $\mathbf{S}_{1357} = \mathbf{S}_{15} + \mathbf{S}_{37}$, $\mathbf{S}_{26} = \mathbf{S}_2 + \mathbf{S}_6$, $\mathbf{S}_{48} = \mathbf{S}_4 + \mathbf{S}_8$, $\mathbf{S}_{2468} = \mathbf{S}_{26} + \mathbf{S}_{48}$, $\mathbf{S}_{12345678} = \mathbf{S}_{1357} + \mathbf{S}_{2468}$, and $\mathbf{S} = \mathbf{S}_9 + \mathbf{S}_{12345678}$. The resulting factorization of the Hilbert space is given in Table 1 (further details of the factorization procedure are given in the Supporting Information). The dimension of the largest matrix is now reduced to 12 486, which is still rather large but can be well handled on present day personal computers with 2 GB of memory storage. A single calculation for one set of the parameters J_R and J_C requires about 2 days on a modern personal computer with 2 GB of RAM.

Table 1. Classification Scheme for the Mixed-Valent Manganese [3 × 3] Grid 1 in the D_4 Symmetry Group

S	A_1	A_2	B_1	B_2	E	total
1/2	2032	1990	2011	2006	4013	16065
3/2	3828	3747	3794	3781	7575	30300
5/2	5212	5095	5162	5149	10291	41200
7/2	6052	5908	5991	5969	11960	47840
9/2	6340	6174	6263	6246	12486	49995
11/2	6100	5925	6025	6000	12025	48100
13/2	5482	5302	5402	5385	10757	43085
15/2	4603	4432	4529	4506	9035	36140
17/2	3647	3485	3571	3557	7103	28466
19/2	2704	2563	2642	2625	5267	21068
21/2	1897	1772	1840	1831	3648	14636
23/2	1240	1140	1195	1185	2380	9520
25/2	768	685	727	723	1436	5775
27/2	436	376	408	404	812	3248
29/2	235	189	213	212	415	1679
31/2	113	84	99	98	197	788
33/2	53	33	42	42	80	330
35/2	20	10	15	15	30	120
37/2	8	2	5	5	8	36
39/2	2	0	1	1	2	8
41/2	1	0	0	0	0	1

A full least-squares fitting of the magnetic susceptibility data, in which both J_R and J_C are allowed to vary independently, is thus unrealistic. However, it is possible within a reasonable time frame to fit the susceptibility data with Hamiltonian (1) for a fixed ratio of J_C/J_R: The Hamiltonian is rewritten as $H = -J_R[H_R + (J_C/J_R)H_C]$, with obvious meanings of H_R and H_C, and the energy spectrum is calculated for $J_R = 1$ and a given ratio J_C/J_R. The energy spectrum for any value of J_R is then obtained by simply scaling the calculated energy values by J_R. The susceptibility is then easily determined via the Van Vleck equation (see eq 2; second-order terms do not appear here since an isotropic model is considered). Thus, a best-fit value for J_R can be obtained with standard least-squares fitting routines, once the energy spectrum for a fixed ratio of J_C/J_R has been calculated.

(13) Waldmann, O. *Phys. Rev. B: Condens. Matter Mater. Phys.* **2000**, *61*, 6138.

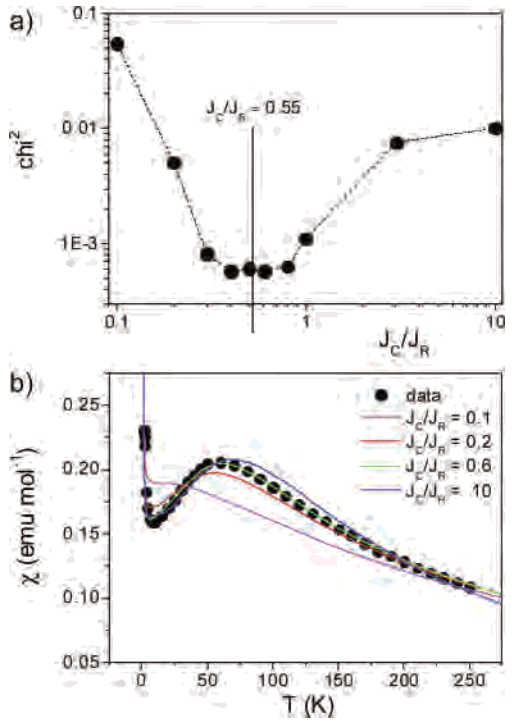

Figure 3. (a) GOF parameter χ^2 as function of the ratio J_R/J_C (for details see text); (b) comparison of the experimental $\chi(T)$ curve (circles) with the best-fit results for the indicated values of J_R/J_C (solid lines).

To obtain best-fit values for both J_R and J_C, a two-step procedure was followed. In the first step, the energy spectrum was calculated for a number of values for J_C/J_R (specifically 0.1, 0.2, 0.3, 0.4, 0.5, 0.6, 0.8, 1.0, 3.0, and 10), and the susceptibility data were least-squares fitted to the model

$$\chi(T) = \frac{N_A \mu_B{}^2 g^2}{3k_B T} \frac{\sum_{S\alpha}(2S+1)S(S+1)\exp[-J_R E_{S\alpha}{}^0/(k_B T)]}{\sum_{S\alpha}(2S+1)\exp[-J_R E_{S\alpha}{}^0/(k_B T)]} + \chi_0 \quad (2)$$

Here, the three parameters J_R, g, and χ_0 were allowed to vary independently. In eq 2, the sum runs over all spin levels, numbered by S and α, and $E_{S\alpha}{}^0$ refers to the energies of the spin levels for a given value of J_C/J_R. The constant χ_0 accounts for a small diamagnetic background due to the grease in the sample. Plotting the goodness-of-fit (GOF) parameter χ^2 as function of J_C/J_R then reveals a best-fit value for J_C/J_R. This way one obtains the best-fit values for J_R and J_C independently. To estimate their confidence limits, it is necessary, in a second step, to again least-squares-fit the data for each ratio J_C/J_R but now with the parameters g and χ_0 set to their best-fit values ($g = 2.11$ and $\chi_0 = -0.006$ $cm^3\ mol^{-1}$: it is remarked that the absolute value of the g factor is of little significance in view of the 5% accuracy of the data calibration).[14]

The GOF parameter χ^2 as function of J_C/J_R is shown in Figure 3a. The χ^2 does not exhibit a simple parabolic dependence, as expected for a Gaussian statistical analysis, but instead shows a more troughlike behavior with a "bottom" reaching from $J_C/J_R \approx 0.3$ to about 0.8. The standard procedure of calculating estimated standard deviations (esds) is related to the curvature of the parabola approximating the χ^2 behavior near the minimum.[14] Since the curvature at the bottom is very small, the resulting calculated esds are ridiculously large and thus do not provide reliable estimators for the confidence limits. To give an impression of what the χ^2 values refer to, the corresponding susceptibility curves are drawn for some of the of J_C/J_R ratios in Figure 3b. For χ^2 values outside the trough, the susceptibility curves clearly deviate from the experimental data, but for J_C/J_R values within the trough, the curves are statistically indistinguishable. Accordingly, $J_C/J_R = 0.55(10)$ is estimated, and with the best-fit value of $J_R = -12$ K for this ratio, this finally translates into

$$J_R = -12(1)\ \text{K} \qquad J_C = -6.5(10)\ \text{K} \quad (3)$$

The susceptibility curve corresponding to these values (and the g and χ_0 values given above) reproduces the experimental data very well (see Figure 2a).

For an isotropic Hamiltonian, such as Hamiltonian (1), the magnetic moments for arbitrary temperature and magnetic fields can also be calculated exactly from the zero-field energy spectrum,[13]

$$m(T,B) = \mu_B g \frac{\sum_{S\alpha} S B_S(gSx)\sinh[g(S+{}^1/_2)x]\exp[-E_{S\alpha}/(k_B T)]}{\sum_{S\alpha}\sinh[g(S+{}^1/_2)x]\exp[-E_{S\alpha}/(k_B T)]} \quad (4)$$

where $B_S(y)$ is the Brillouin function, $x = \mu_B B/(k_B T)$ and $E_S\alpha$ denotes the energy levels (in this work $E_{S\alpha} = J_R E_{S\alpha}{}^0$). It is easily confirmed that for $B \rightarrow 0$, eq 4 reduces to the Van Vleck equation for the susceptibility. Equation 4 enables the calculation of the magnetization curve, and the result is in excellent agreement with experiment (Figure 2b). The calculated energy spectrum yields an $S = {}^1/_2$ ground state of the cluster, in agreement with the data, and an $S = {}^3/_2$ level at 9.5 K, which explains the upturn of the $m(B)$ curve at higher fields. Thus, as a conclusion, the obtained best-fit values reproduce the magnetism of **1** very well. With a Hilbert space of dimension 4 860 000, this is to date by far the largest system for which a full quantum mechanical analysis of the magnetization curves could be achieved.

On general grounds it cannot be assumed that magnetic anisotropy terms in the microscopic spin Hamiltonian, for instance due to ligand−field or dipole−dipole interactions, are negligible.[3,15] However, in the present case their effects are hardly seen in measurements on powder (or polycrystalline) samples. On one hand, effects of the anisotropy are detectable only at the lowest temperatures, since at higher temperatures, as soon as an appreciable number of levels

(14) Press, W. H.; Flannery, B. P.; Teukolsky, S. A.; Vetterling, W. T. *Numerical Recipes. The Art of Scientific Computing;* Cambridge University Press: Cambridge, U.K., 1986.

(15) Waldmann, O.; Zhao, L.; Thompson, L. K. *Phys. Rev. Lett.* **2002**, *88*, 066401.

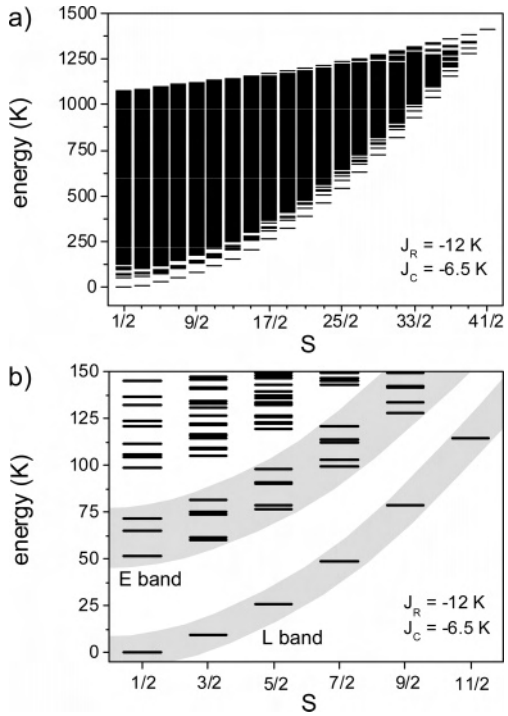

Figure 4. Energy spectrum versus total spin quantum number S as calculated from Hamiltonian (1) with the parameters indicated in the panels: (a) full energy spectrum; (b) detailed view on the low-energy sector, highlighting the L band ($\hat{=}$ quantized rotation of the Néel vector) and E band ($\hat{=}$ quantized spin wave excitations).

become thermally populated, the anisotropy effects average out. On the other hand, the $S = {}^1/_2$ ground state of **1** cannot exhibit a zero-field-splitting, that is, the anisotropy is not effective in the ground state. In our opinion, this explains why the simple isotropic Hamiltonian (1) manages to reproduce well both the susceptibility and the magnetization curve.

Discussion

It is interesting to inspect the calculated energy spectrum for **1**. The full spectrum, as a function of S, is shown in Figure 4a, and a more detailed view of the low-energy part is provided in Figure 4b. As mentioned already, the ground state belongs to $S = {}^1/_2$, followed by an $S = {}^3/_2$ state at 9.5 K. The higher-lying levels show a remarkable but well-known structure,[2,4,16,17] where the lowest states for each S exhibit a quadratic increase of energy $\propto S(S+1)$, which is characteristic for rotational bands. The lowest rotational band of states is known as the L band or "tower of states". Furthermore, the next-higher lying states above the L band form another set of rotational bands, also showing the typical $S(S+1)$ increase in energy. This set of rotational bands has been collectively denoted as the E band.

A comparison shows that the spectrum of **1** looks very similar to that of the antiferromagnetic wheels or the "original" Mn(II)-[3 × 3] grid.[2,4,17] In fact, its low-lying energy levels exhibit all the characteristic features found in these systems. The main difference is that in **1** the L band starts from $S = {}^1/_2$, whereas it starts from $S = 0$ in the case of the wheels and $S = {}^5/_2$ in the case of Mn(II)-[3 × 3]. The similarity has the important implication that the spin dynamics and elementary magnetic excitations, respectively, in **1** are explained by the same physical picture as in the wheels and Mn(II)-[3 × 3].[2,4] In this picture, the L band corresponds to the (quantized) rotation of the Néel vector, and the E band corresponds to the (quantized) spin-wave excitations. It has become clear in recent years that this structure of the low-energy part of the spectrum is intimately connected to a "classical" spin structure.[2,4,17] Indeed, the $S = {}^1/_2$ ground state can be easily rationalized by the classical spin configuration shown in Figure 1c.

These considerations implicitly demonstrate that the spin dynamics in **1** at the lowest temperatures are well described in terms of a Néel vector (the Néel vector is simply a vector which is parallel to the magnetization of one of the antiferromagnetic sublattices, e.g., to the up-pointing spins in Figure 1c). Thus, if the magnetic anisotropy is of the easy-axis type and large enough, and the Mn(III) ions are known to be good sources for easy-axis magnetic anisotropy, **1** would be in the regime of quantum tunneling of the Néel vector.[18,19] A careful determination of the magnetic anisotropy of **1** will be thus of high interest. As an additional comment, the classical spin structure also ensures that the effective (three-sublattice) spin Hamiltonian

$$H_{AB9} = -J'_R \mathbf{S}_A \cdot \mathbf{S}_B - J'_C \mathbf{S}_B \cdot \mathbf{S}_9 \qquad (5)$$

developed for the Mn(II)-[3 × 3] grid works well also for **1**.[19] In eq 5, A and B refer to the two magnetic sublattices formed by the edge and corner spins, that is, $\mathbf{S}_A = \mathbf{S}_{1357}$, $\mathbf{S}_B = \mathbf{S}_{2468}$ (where $\mathbf{S}_A$ and $\mathbf{S}_B$ assume their maximal values $S_A = S_1 + S_3 + S_5 + S_7$, $S_B = S_2 + S_4 + S_6 + S_8$; therefore $S_A = 8$ and $S_B = 10$ for **1**). Physically, this means that the low-energy dynamics corresponds to a motion in which the spins on each of the sublattices A and B act as a single, larger spin.

It is also interesting to look at **1** from another perspective, which is suggested by its $S = {}^1/_2$ ground state. A spin-$^1/_2$ is a natural candidate for a quantum bit (qubit), the basic element of a quantum computer. However, among the many obstacles to be overcome in the realization of a quantum computer is the problem of addressing the qubit, which is a prerequisite for its initialization and read-out. For conventional spin-$^1/_2$ systems, in which the spin-$^1/_2$ arises from one unpaired electron, addressing is extremely difficult because of the typical smallness of the objects. However, recently it has been argued that mesoscopic spin-$^1/_2$ systems, in which the spin-$^1/_2$ arises from the concerted action of many electrons (41 in the case of **1**), might be good candidates for producing qubits (then called cluster qubits), because their larger physical size simplifies the task of addressing accordingly.[11]

A molecule discussed much in this context is the Cr_7Ni wheel.[9−12] In this wheel, the eight metal centers are arranged

(16) Schnack, J.; Luban, M. *Phys. Rev. B: Condens. Matter Mater. Phys.* **2001**, *63*, 014418.
(17) Waldmann, O. *Phys. Rev. B: Condens. Matter Mater. Phys.* **2002**, *65*, 024424.
(18) Chiolero, A.; Loss, D. *Phys. Rev. Lett.* **1998**, *80*, 169.
(19) Waldmann, O. *Phys. Rev. B: Condens. Matter Mater. Phys.* **2005**, *71*, 094412.

as an almost perfect ring and exhibit next-neighbor antiferromagnetic interactions. Because of the smaller spin of the Ni(II) ion (spin-1) as compared to the Cr(III) centers (spin-$^3/_2$), the ground-state spin configuration is not fully compensated, resulting in an $S = {}^1/_2$ ground state. The next-higher lying state, an $S = {}^3/_2$ level, is at about 13 K above the ground state. Detailed numerical calculations and theoretical considerations have shown that the $S = {}^1/_2$ cluster ground state of Cr_7Ni indeed may provide a qubit, that is, that the leakage to the nearby $S = {}^3/_2$ levels is small enough, et cetera.[12]

The above discussion has shown that the classical spin structure in **1** also means that the effective three-sublattice spin Hamiltonian concept describes the low-lying excitations well. Furthermore, in ref 19 it has been demonstrated that for $J_C \gtrsim 0.01J_R$ the sublattice spin S_B and the central spin S_9 are so strongly coupled that they act as a combined spin. As a result, the three-sublattice spin Hamiltonian can be further reduced to another effective spin Hamiltonian, which is exactly the effective spin Hamiltonian of a modified antiferromagnetic wheel. Thus, magnetically, **1** behaves at low temperatures exactly like a modified wheel with an $S = {}^1/_2$ ground state, that is, like Cr_7Ni. Also the energy gaps to the next-higher lying $S = {}^3/_2$ are on the same order (9.5 K in **1** and 13 K in Cr_7Ni). The considerations drawn for Cr_7Ni in the context of the applicability as cluster qubits[12] thus are valid also for **1**. In short, the mixed-valent manganese [3 × 3] grid **1** might be another system with significant potential as a cluster qubit. Recently, it has been shown that suitably functionalized manganese [3 × 3] grids can be organized in monolayers of surface-bound molecules onto substrates, for example, Au(III), and can be individually addressed by scanning probe techniques,[6] overcoming another prerequisite for their application.

Acknowledgment. Partial financial support from the EC-RTN-QUEMOLNA, Contract N*o*. MRTN-CT-2003-504880, the Natural Sciences and Engineering Research Council of Canada, and the Swiss National Science Foundation is gratefully acknowledged.

Supporting Information Available: Details of factorization of the Hilbert space. This material is available free of charge via the Internet at http://pubs.acs.org.

IC052055D